Research article

Cuproptosis combines immune landscape providing prognostic biomarker in head and neck squamous carcinoma

Tingting Shu [a,b], Xudong Wang [a,b,*]

[a] Department of Maxillofacial and Otorhinolaryngological Oncology, Tianjin Medical University Cancer Institute and Hospital, National Clinical Research Center of Cancer, Tianjin, 300060, China
[b] Tianjin's Clinical Research Center for Cancer, Tianjin, 300060, China

A R T I C L E   I N F O

A B S T R A C T

Head and neck squamous carcinomas (HNSC) are the seventh most common cancer around the world. Treatment options available today have considerable limitations in terms of efficacy. Identifying novel therapeutic targets for HNSC is, therefore, urgently needed. As a novel determined regulated cell death (RCD), Cuproptosis is correlated with the development, treatment response, and prognosis of various cancer. However, the potential role of Cuproptosis-related genes (CRGs) in the tumor microenvironment (TME) of HNSC remains unclear. To figure out whether TME cells and Cuproptosis could better predict prognosis, in this study, we analyzed the expression, mutation status, and other clinical information of 502 HNSC patients by dividing them into four clusters based on their CRGs and TME cell expression. Utilizing the LASSO-Cox method and bootstrap, we established Prognostic Cuproptosis and TME classifier, which were significantly associated with prognosis, pathways, clinical features, and immune cell infiltration in TME of HNSC. To go further, the subgroup Cup low/TMEhigh displayed a better prognosis than any others. Two GEO datasets demonstrated the proposed risk model's clinical applicability. Our GO enrichment analyses proved the conjoint effect of Cuproptosis and TME on tumor angiogenesis, proliferation, and so on. Single-cell analysis and Immunotherapy profile then provided a foundation for determining the molecular mechanisms. It revealed the prognostic risk score positively correlated with T cell activation and natural killer (NK) recruiting. As far as we know, this study is the first time to explore the involvement of CRGs regulation in the TME of HNSC. In a word, it is vital to use these findings to develop new therapeutic strategies.

1. Introduction

Head and neck squamous carcinomas (HNSC) take up 90% of all head and neck cancers and will remain among the leading causes of cancer incidences and deaths until 2020 [1]. Traditional treatments often result in severe physiologic and psychological complications [2]. Further, surgical removal of the tumor reduces physical function, and many patients suffer recurrences and metastases due to the surgery [3]. In recent years, significant advancements have been made in developing HNSC therapeutic approaches, including immunotherapy, targeted therapies, and some combination means [4]. We all know that immunotherapy has brought new ideas and

* Corresponding author. Tianjin Medical University Cancer Institute and Hospital, Department of Maxillofacial & E.N.T, Tianjin' Clinical Research Center for Cancer, National Clinical Research Center for Cancer, Key Laboratory of Cancer Prevention and Therapy, Tianjin, China.
E-mail address: wxd.1133@163.com (X. Wang).

hope for the clinical treatment of head and neck squamous cell carcinoma. However, it should note that the Objective Response Rate (ORR) of immunotherapy still needs to be improved. Hence, we need to find more prognostic targets for this disease.

Cuproptosis is a recently uncovered nonapoptotic programmed cell death discriminated acknowledged death mechanisms. Protein lipoylation mainly triggers copper production and copper combined with lipoylated elements of the TCA during Cuproptosis. Following previous reports, this phenomenon has also been observed in HNSC [5–9].

Thus, our study aimed to link Cuproptosis to the TME in head and neck squamous carcinomas to develop a Cup-TME classifier for therapeutic response prediction and prognostic. We hope that our method can provide an approach to improve the prediction of the immunotherapy response.

2. Materials and methods

2.1. Data source and preprocessing

HNSC data were downloaded from TCGA. Furthermore, GSE41613 dataset with the platform GPL570 and its clinical information were acquired from GEO. Single-cell expression data were collected from GSE172577 to explore TME and Cuproptosis in each cell. Otherwise, we choose GSE42743 and GSE31056 to evaluate our model's effectiveness and generalization ability. For TCGA-HNSC expression data, we only keep tumor-related specimens. Next, we collected and integrated 398 potential Cuproptosis-related genes from the preceding literature [10](Table S1).

2.2. Immune cell infiltration analysis

Using RNA profiles, the CIBERSORT website (https://cibersort.stanford.edu) gives type information about immune cells [11]. It is a deconvolution algorithm which derives a p-value for the deconvolution of each sample and $p < 0.05$ was considered accurate. We used this method to examine the immune infiltration in the head and neck squamous carcinoma tissue in our investigation.

2.3. Identification of overall prognostic Cuproptosis-related genes and immune cells

By using univariate Cox regression method, our study recognized factors connected with Cuproptosis that were noticeably associated with OS of HNSC ($P < 0.05$, FDR<0.05). Subsequently, more valuable prognostic factors were screened by LASSO. Furthermore, we applied multiple-Cox analysis to pick the most valuable prognostic indicator and using Bootstrap sampling to obtain robustness of predictors from it [12]. This procedure was repeated 10,000 times and we got 10,000 cox regression model which was employed to figure out the frequency of each feature that was enrolled in this predictive model. Later, we obtained an overall prognostic value of TME cells with the same method. The overall prognostic value of Cuproptosis-related genes and TME cells was described by hazard ratio (HR) and their 95% CI (confidence interval). Finally, we selected 14 Cuproptosis-related genes (Table S2) and 6 TME cells (Table S3).

2.4. Establishment of Cup-TME classifier

We calculated scores using the formula:

$$\textbf{Cup\_score} = \sum_{i=1}^{n1} \textbf{\textit{boot\_coef}}_i \; x \; \textbf{\textit{Exp}}_i$$

$$\textbf{TME\_score} = \sum_{j=1}^{n2} \textbf{\textit{boot\_coef}}_j \; x \; \textbf{\textit{Exp}}_j$$

where Exp_i or Exp_j are the expression levels of each Cuproptosis-related genes or TME cells. $boot\_coef_i$ or $boot\_coef_j$ are calculated by coef/sd (bootstrap) (coef obtained from multiple cox regression and sd (bootstrap) getting from the standard deviation of bootstrap). Then these two scores are used for construct a Cup-TME classifier. We divide the classifier into four group: Cup^{low}/TME^{high}, Cup^{low}/TME^{low} and Cup^{high}/TME^{high} and Cup^{high}/TME^{low} in reference to the mean of TME_score and Cup_score [13].

2.5. Functional enrichment analysis

Symbol ids of the Differentially expressed genes (DEGs, p-value<0.05, |logFC| > 1,FDR<0.05) were turned to entrez ids using the R package "org.Hs.eg.db." [14]. Through the "clusterProfiler" R package, DEGs were then analyzed using GO enrichment analysis and KEGG analysis, P value < 0.05 after correction was used as the thresholds [15,16]. According to 'clusterProfiler' and 'fgsea' packages, GSEA and FGSEA were implemented using the hallmark gene set (c2.cp.kegg.v7.5.1.entrez.gmt) in MSigDB database. Adjusted *P*-value <0.05 was recognized to be statistically significant [17].

2.6. WGCNA

WGCNA, a bioinformatic approach, discover exceedingly coadjuvant genes and can analyze those which have highly linkage to

disease. A module's highly interconnected hub genes were considered functionally significant genes. Here, WGCNA was used to recognized hub modules [18,19]. And Cytoscape software was used to screen hub genes [20]. In order to further analyze and validate the hub genes from the WGCNA, common hub modules were identified.

2.7. Tumor somatic mutation analysis

Tumor mutation data of TCGA-HNSC were available in the TCGA database. R package "ComplexHeatmap" was used to draw Oncoprints [21]. Using "limma" package in R to conduct DEGs analysis [22]. In addition, Proteomaps, a web approach, were drew on account of the DEGs.
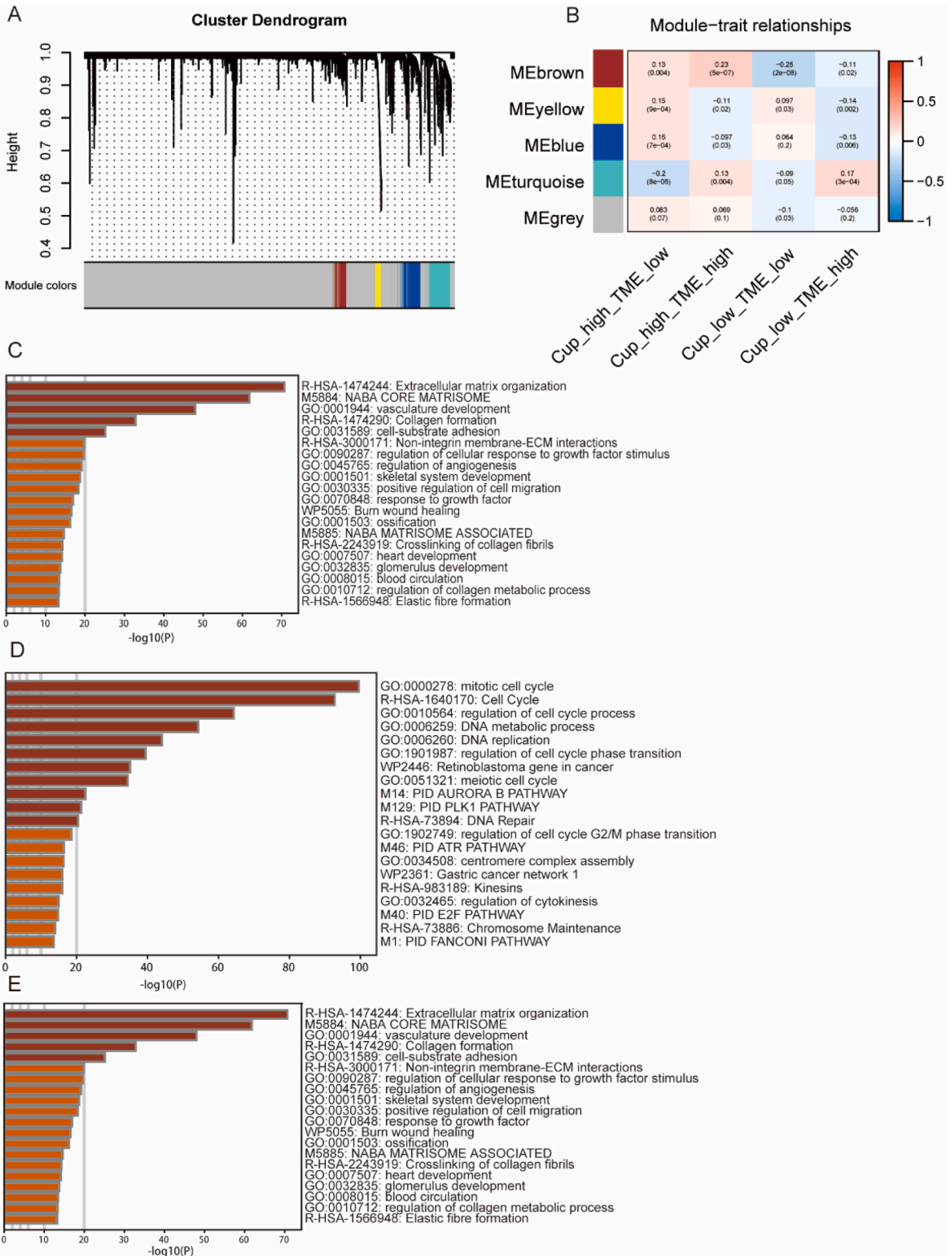
2.8. Cell-cell communication analysis

Cell–cell communication was studied by the R package 'CellChat' (v1.5.0) [23]. By means of establishing CellChat objects, we put the Secreted Signalling pathway as the reference database and identify putative interaction pairs.
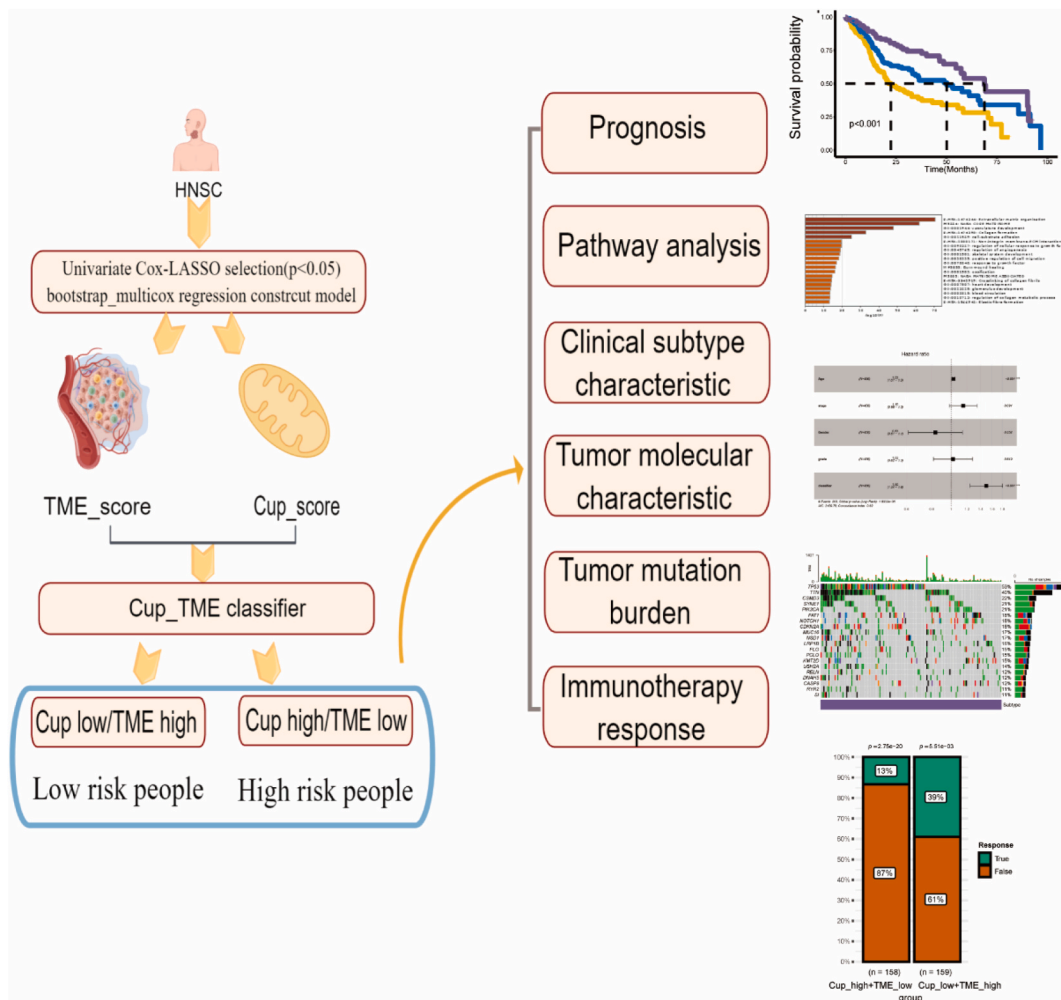
Fig. 1. The construction and validation of Cup-TME model. Independent HNSC patient's cohort with complete clinical information, TCGA-HNSC, which were used to establish the prognostic TME score and Cuproptosis score, respectively. Bootstrap-multicox regression analyses of 22 TME cells and 398 Cuproptosis-related genes were performed. In the end, we got 6 TME cells. As well, 14 Cuproptosis-related genes were used for the establishment of Cuproptosis score. A Cup-TME classifier which integrated the TME and Cuproptosis scores classified all patients into three different subgroups: Cup^{low}/TME^{high}, mixed, and Cup^{high}/TME^{low}. Based on the Cup-TME classifier, the differences in prognosis, pathway enrichment analysis, clinical subtype features, tumor mutational burden, and tumor molecular characteristics were investigated in several patient subgroups. Another independent cohort (GSE42743 and GSE31056) were used to further validate the classifier's performance.
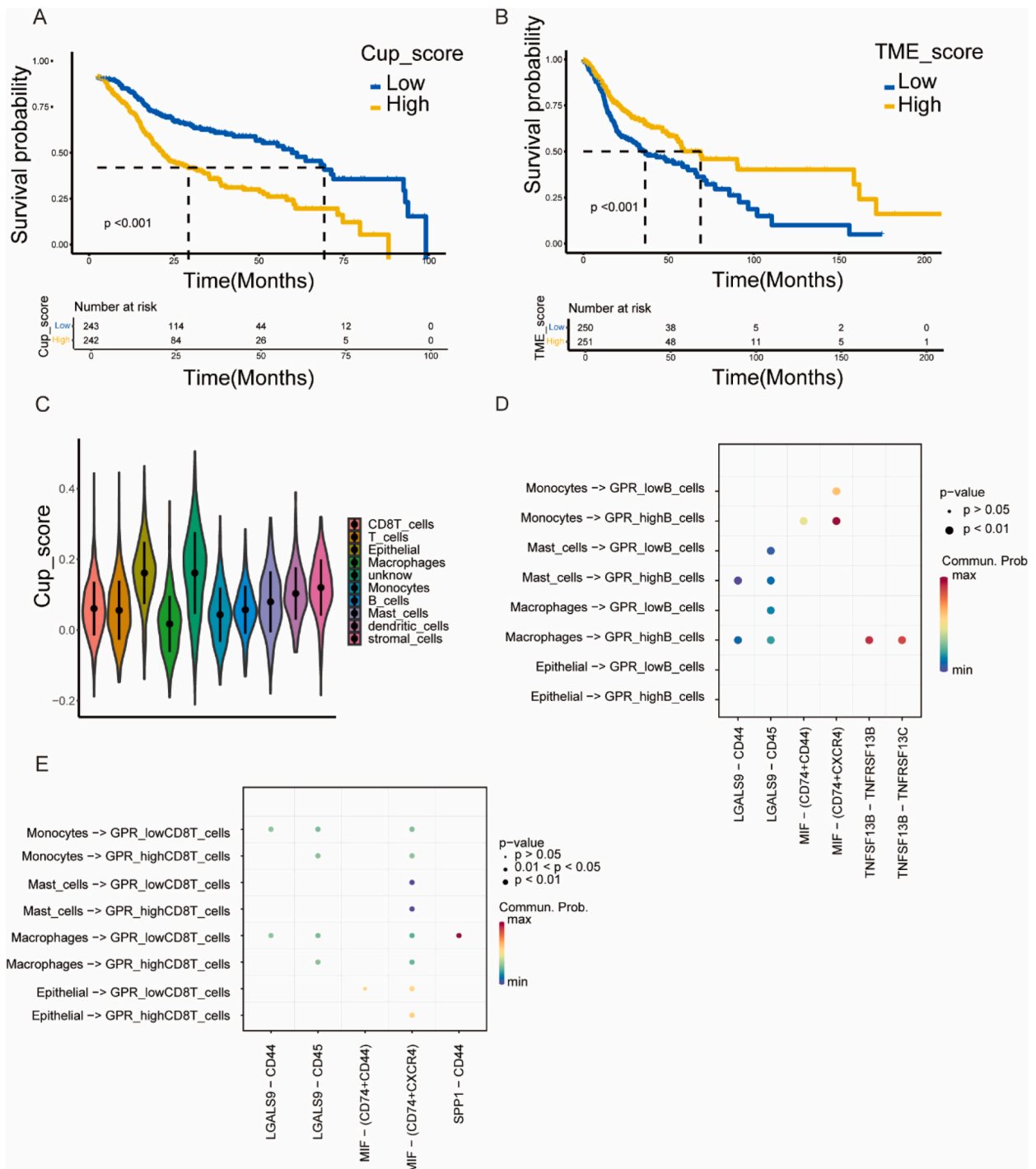
Fig. 2. The construction of the Cuproptosis Scoring (Cup-score) model and TME-score model. (A). Kaplan-Meier survival analysis of the two strata. Patients with high Cup-score HNSC had a worse prognosis. The yellow line represents the high Cup-score, and the blue line represents the low Cup-score. P < 0.001 (B). Kaplan-Meier survival analysis of patients with low TME-score had a worse prognosis. The yellow line represents the high TME-score, and the blue line represents the low TME-score. P < 0.001 (C). Violin plot shows that Cup_score is differentially expressed in different cell types. (D), (E). Bubble plots show ligand-receptor pairs difference. P < 0.01 was considered significant. (For interpretation of the references to color in this figure legend, the reader is referred to the Web version of this article.)

A — Cluster Dendrogram

B — Module−trait relationships

C — R-HSA-1474244: Extracellular matrix organization ... R-HSA-1566948: Elastic fibre formation

D — GO:0000278: mitotic cell cycle ... M1: PID FANCONI PATHWAY

E — R-HSA-1474244: Extracellular matrix organization ... R-HSA-1566948: Elastic fibre formation

(caption on next page)

Fig. 3. Identification of modules associated with the clinical traits of head and neck cancer. (A). Dendrogram of all differentially expressed genes clustered based on the measurement of dissimilarity (1-TOM). The color band shows the results obtained from the automatic single-block analysis. (B). Heatmap of the correlation between the module eigengenes and subgroups of HNSC. We selected the MEblue, MEyellow and MEbrown block for subsequent analysis. (C), (D), (E). Functional enrichment analysis for the hub genes in the royal blue, yellow and brown module by Metascape analysis, respectively. (For interpretation of the references to color in this figure legend, the reader is referred to the Web version of this article.)

2.9. TIDE analysis

TIDE is a bioinformatic analysis to forecast immunotherapeutic responses [24]. We submitted the transcriptome data of patients from the TCGA-HNSC cohort to this website (http://tide.dfci.harvard.edu) and downloaded the result.

2.10. Potential sensitive drug prediction

We used the "oncoPredict" R package to predict the sensitivity of HNSC patients to common chemotherapeutics in the TCGA cohort with different subgroups [25]. Drug sensitivity data were downloaded from the CTRP.

2.11. Statistical analysis

R version 4.1.2 was undertaken for statistical analysis. Fisher's test was used to calculated Categorical variables. The Wilcoxon test was applied to contrast continuous variables between two groups. R package "ggplot2" was used to visualize data [26]. *, $P < 0.05$; **, $P < 0.01$; ***, $P < 0.001$. $P < 0.05$ was considered statistically significant.

3. Result

3.1. Identification of prognostic of Cuproptosis and TME in the TCGA cohort

The workflow of this research is summarized in Fig. 1. In the TCGA cohorts, 398 Cuproptosis-related factors and 22 types of TME cells were independently examined to determine prognosis. 398 gene signatures were analyzed using univariate Cox regression and LASSO. Later, we used Multivariate Cox analysis to develop the Cuproptosis-signature. Bootstrap sampling was used to obtain the robustness of predictors to make them more credible. In the end, 14 potential Cuproptosis-related genes (APP, COPZ1, PSMB5, SLC7A5, ARF1, STK11, SLC25A5, DOT1L, RSL1D1, TKT, AQP1, MT2A, SLC25A51, MTIF3) were identified. None of these genes have previously been reported in patients with head and neck squamous cell carcinoma. We calculated all the Cuproptosis Score (Cup_score) for every HNSC patient and then applied the same approach to TME and obtained 6 significantly important TME cells. TME_score was also calculated. Next, we analyzed the performance of Cup_score and TME_score in the TCGA cohort (Fig. 2A, 2B) . We can see lower Cup_score and higher TME_score hold better clinical outcomes. As a significant step toward further validating the Cuproptosis and TME scores, we analyzed single-cell data from oral cancer samples. And we noticed that CD8 T cells or T cells, dendritic cells, are consistently positively correlated with Cup_score, which implied why we could use this Cup_score and why it is often associated with TME (Fig. 2C). It provides us with solid arguments. Different subgroups of patients may also be affected by cell and cell communication in addition to intrinsic cell information. Subsequently, we found that there was frequent communication between Macrophages and Cup_lowCD8T_cells. According to our findings, Cup_lowCD8T_cells primarily receive signals from monocytes, macrophages, and ligand-receptor pair analysis revealed that macrophages prefer to send signals to immunocytes by SPP1–CD44. SPP1–CD44 has been demonstrated to play a pivotal role in many kinds of tumors during previous studies [27–30]. And it has been shown that the high infiltration of SPPI + macrophages reduce the response to immunotherapy. This suggests that combining immunotherapy of these two targets may have good results in these Cup_lowCD8T_cells patients. We similarly explored the role of B cells. We also observed that the biological functions of Cup-highB_cells and Cup-lowB_cells are different. Taken together, compared with Cup_high immune cells, Cup_low is likely to communicate more with immune cells [31–35] (Fig. S1, Fig. 2D and E).
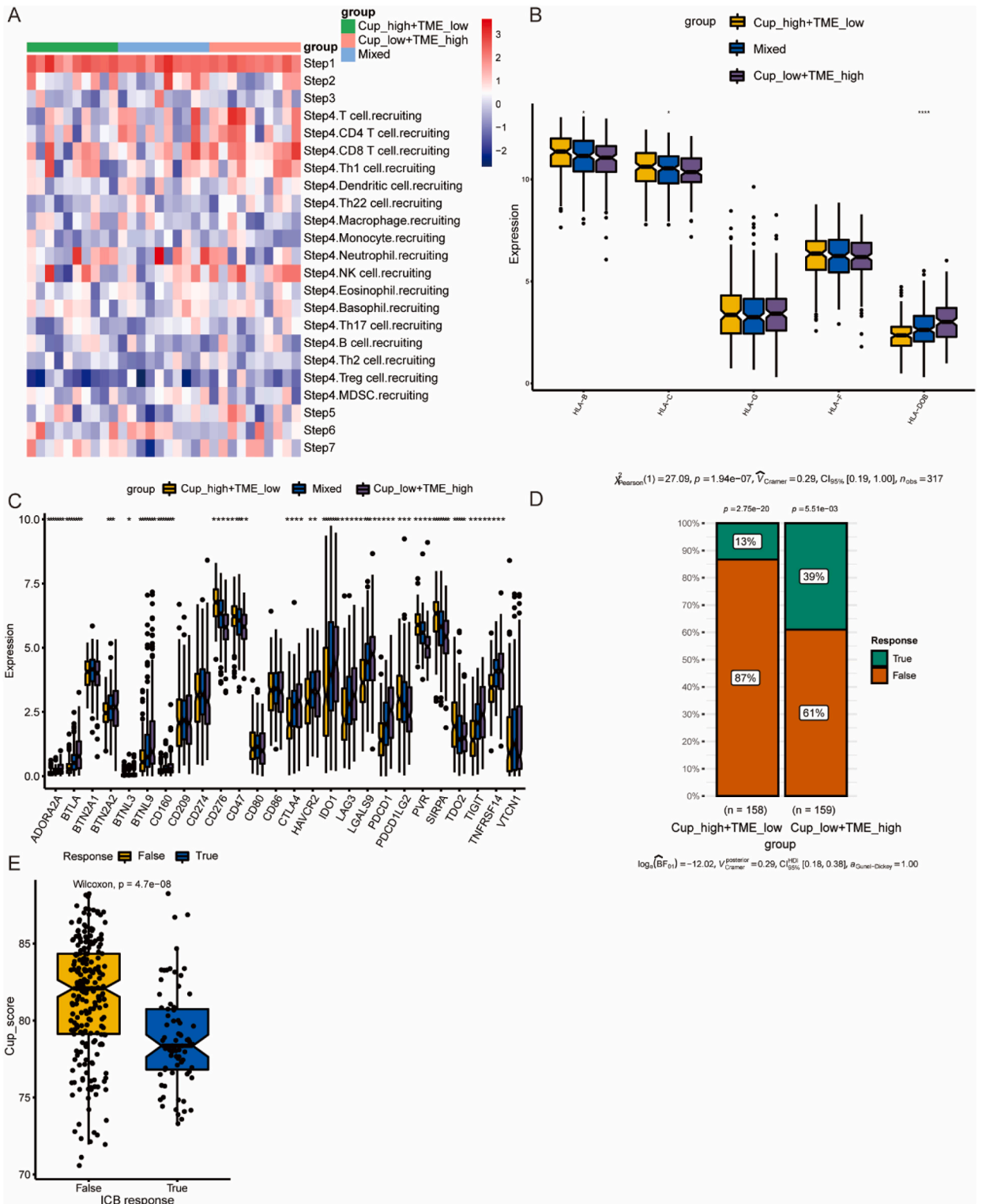
3.2. Functional analysis among different Cuproptosis -TME subgroups

Considering the effectivity, we next asked what the effect would be if we combined both scores. We combined the Cup_score and TME_score, resulting in four subgroups: Cup^{low}/TME^{high}, Cup^{low}/TME^{low}, Cup^{high}/TME^{high} and Cup^{high}/TME^{low} (Fig. S2). KEGG analyses showed that high Cup_score manifested a much higher enrichment of cell cycle , ECM-receptor interaction, and cell adhesion than tumors with a low Cup_score. Furthermore, higher TME_score displayed up-regulated immune pathways, like antigen processing and presentation, NK cell-mediated cytotoxicity, T cell receptor signaling pathway, cytokine receptor interaction, and others. The results suggest increased antitumor immunity with high TME_score, and patients who belong to this subgroup showed inhibition of tumor growth. In addition, these also proved that Cuproptosis and TME exert synergistic effects on the metabolism of tumors and the proliferation of tumors (Figs. S3 and 4).

For searching differences among different Cuproptosis-TME subgroups. We used WGCNA and set soft threshold (β) = 21 to ensure a scale-free network. We found that blue, brown, and yellow modules exhibited a negative correlation with Cup^{low}/TME^{high} and a
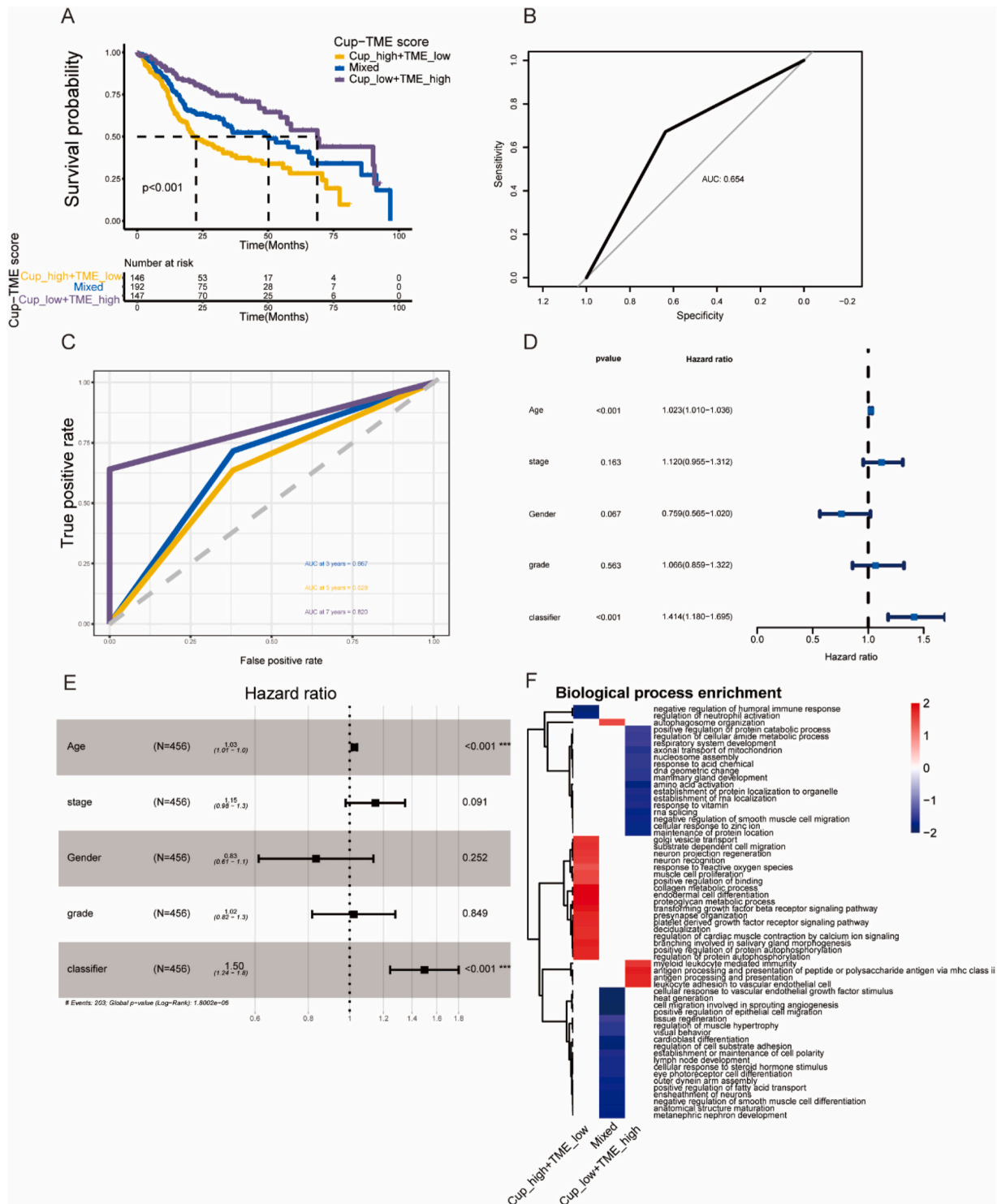
Fig. 4. The construction and validation of the Cup-TME classifier. (A). Kaplan-Meier overall survival curves of TCGA-HNSC training cohorts (n = 502) divided into three different subgroups based on the Cup-TME classifier. Log-rank test, P < 0.001. (B). Prognostic efficiency ability evaluation of this model by introducing the receiver operating characteristic (ROC) curve. (C). Time-dependent ROC curves at separately three year, five years, and seven years. (D), (E). The forest plot shows the results of the univariate Cox regression analysis and multivariate cox analysis, respectively. (F). FGSEA reveals main regulated pathways of the differences in the Cup-TME classifier.

$\chi^2_{Pearson}(1) = 27.09, p = 1.94e{-}07, \widehat{V}_{Cramer} = 0.29, CI_{95\%} [0.19, 1.00], n_{obs} = 317$

$\log_e(\widehat{BF}_{01}) = -12.02, V^{posterior}_{Cramer} = 0.29, CI^{HDI}_{95\%} [0.18, 0.38], a_{Gunel-Dickey} = 1.00$

(caption on next page)

Fig. 5. Comparison of immune-related markers and therapy responses prediction based on Cup-TME classifier. (A). The 23 normalized immune activity scores obtained by TIP. (B) HLA gene-set is differentially expressed between these subtypes. (C). The immune checkpoint gene-set is differentially expressed between these subtypes. (The Cup^{low}/TME^{high}, mixed and Cup^{high}/TME^{low} subgroups are represented as purple, blue and yellow, respectively.) (D). The different percentages of immunotherapy responder among Cup^{low}/TME^{high} and Cup^{high}/TME^{low} based on Cup-TME classifier. (E). Comparison of Cup-scores between immunotherapy responder and nonresponder. (For interpretation of the references to color in this figure legend, the reader is referred to the Web version of this article.)

positive correlation with Cup^{high}/TME^{low}. Consequently, we applied these modules to the Metascape database [36], performing GO and KEGG enrichment analyses. Results showed Cup^{high}/TME^{low} remarkably correlated with extracellular matrix organization, vasculature development, and cell-substrate adhesion [37] (Fig. 3A, B, C, D, E).

3.3. Establish and estimate the prognostic value of Cup_TME classifier

To increase the interpretability of the classifier, we merged the Cup^{low}/TME^{low} and Cup^{high}/TME^{high} into Mixed. The Cup-TME classifier manifested a dramatically different prognosis in HNSC cohorts. Kaplan-Meier analysis affirmed the survival disparity among these groups (p < 0.001; Fig. 4A). In addition, the classifier was estimated by ROC and time ROC; the values of AUC for 3-, 5-, and 7-year survival times were 0.667, 0.628, and 0.820, separately using univariate and multivariate Cox regression analysis (Fig. 4B and C). We demonstrated the Cup-TME classifier's prognostic value. The Cup-TME classifier was closely related to overall survival in training cohorts with sufficient patients (Fig. 4D and E). The Cup-TME classifier was applied to FGSEA. And results revealed that Cup^{low}/TME^{high} subgroup was significantly related to antigen processing and presentation, and Cup^{high}/TME^{low} subgroup had a strong correlation with angiogenesis or cell migration, which further illustrated the effectiveness and feasibility of our classification (Fig. 4F).

3.4. Tracking the tumor immunophenotype

Data and pictures of anticancer immune activity were collected from the TIP website. TIP (Tracking Tumor Immunophenotype) consolidates 'ssGSEA' and 'CIBERSORT' to track anticancer immunity [38]. After visualizing with TIP, we found that essential steps are CD8 T cell recruiting, T cell recruiting, and NK cell recruiting in Cup^{low}/TME^{high} subgroup, which also leads to why this subgroup has the best prognosis (Fig. 5A).

3.5. Distinct immune response profile and TMB

In addition, we investigated several aspects of immune response-associated genes toward various subgroups, such as major histocompatibility complex (MHC) and immune checkpoint. Moreover, we can see that the Cup^{low}/TME^{high} subgroup had a higher expression in several MHC (Fig. 5B). As we all know; Immune checkpoints are vital to cancer immune infiltration. Therefore, we analyzed immune checkpoint genes' expression levels among Cup^{high}/TME^{low}, mixed and Cup^{low}/TME^{high} subtypes. Then, we discovered that 13 genes are higher in the Cup^{low}/TME^{high} subtype than the other two subgroups. The 13 genes included ADORA2A, BTN2A2, BTNL9, CD160, CD209, LGALS9, CTLA4, BTLA, LAG3, PD1, TIGIT, TNFRSF14, VTCN1. Many immune checkpoint genes overexpressed in the subtype are promising targets waiting for in-depth research. Some of them have proven their immense value for immune checkpoint blockade therapy such as TIGIT, CTLA4, LAG3 and PD-1 (Fig. 5C). Then, our study focused on elucidating the genetic imprints of each subgroup using the intrinsic correlation between TMB and Cup_score. However, we did not find a significant variation between the subgroups. To a certain extent, these results demonstrated that our model has better sensitivity to discriminate patients. Finally, we investigated the immune response in patients from different groups by the TIDE website. According to expectations, Cup^{high}/TME^{low} patients exhibited a lower response rate, and Cup^{low}/TME^{high} patients exhibited a higher immunotherapy objective response rate (Fig. 5D). We further investigated the impact of Cup_score on outcomes with Immunotherapy for Patients with HNSC (Fig. 5E). We observed that patients in the higher Cup_score subgroups had less immunotherapy response. As a result, Cup^{low}/TME^{high} patients may benefit more from immunotherapies.

Then, by building proteomaps, we could view the diversities between cellular signaling pathways between Cup^{low}/TME^{high} and immunotherapy response group. Interestingly, these two groups of signaling pathways were found to be similar. In some respects, this explains the suitability of the Cup^{low}/TME^{high} group for immunotherapy in terms of the mechanism. The above results further demonstrate the biological implications of the integrated Cup_score and TME score in the TME, to some extent, helping to unravel different subgroups' prognostic differences based on tumor immunology and Implemented precision immunotherapy (Fig. 6E, F, G, H).

3.6. Response to chemotherapy drugs

HNSC is commonly treated with chemotherapy. In order to inquire into the therapeutic effect of chemotherapy drugs for patients with different groups, we further surveyed the sensitivity difference between Cup^{low}/TME^{high} and Cup^{high}/TME^{low}. GDSC database analysis showed that there are many differences in drug sensitivity between these subtypes (Table S4). We discovered that Cup^{high}/TME^{low} group was more sensitive to these chemotherapy drugs. This means group Cup^{high}/TME^{low} is more suitable for chemotherapy than group Cup^{low}/TME^{high}, which is more appropriate immunotherapy according to the previous analysis. We also tried other different methods of integrating the three groups, and the results were the same.
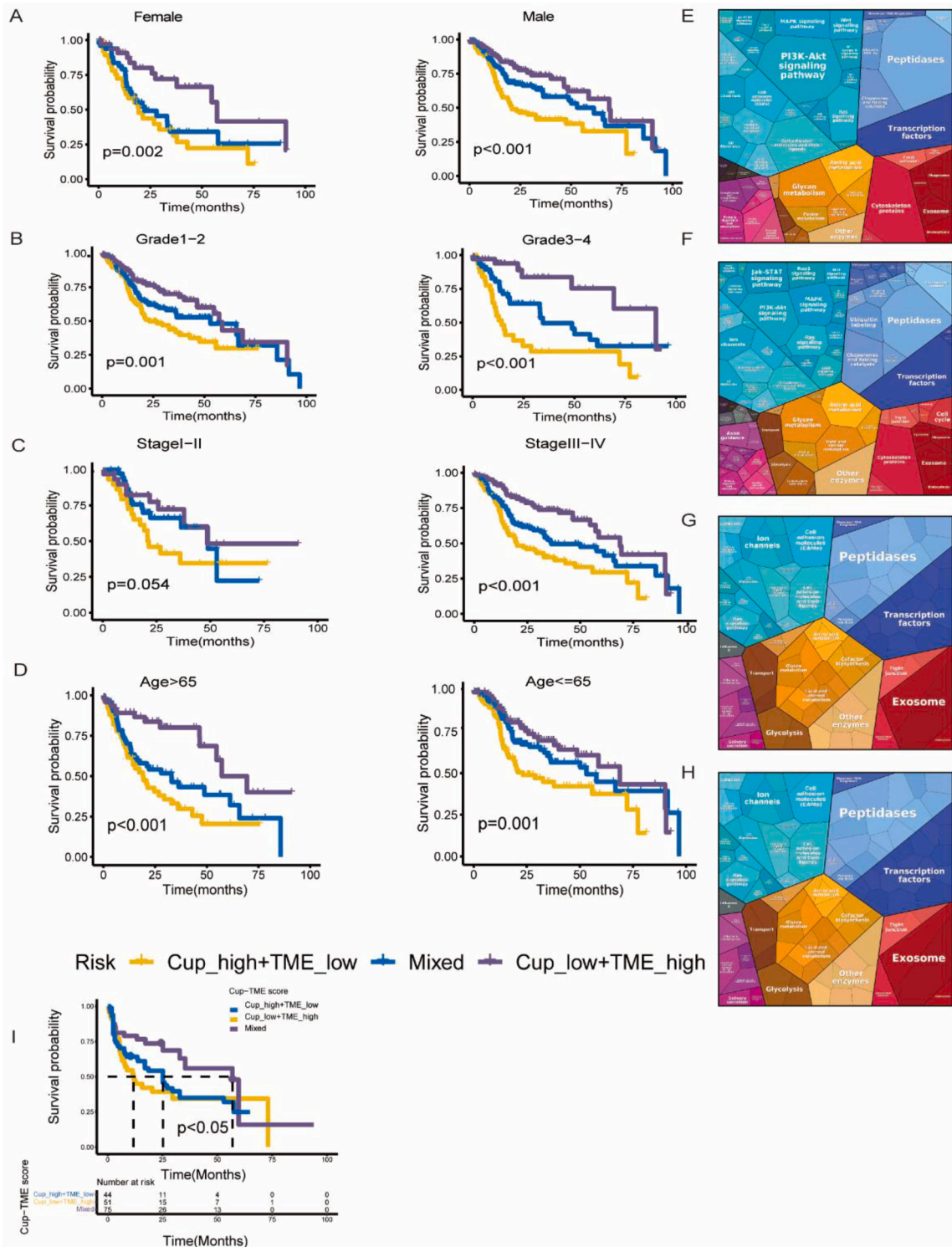
Fig. 6. Survival analysis of the subgroup of clinical factors and functional analysis. (A), (B), (C), (D). Kaplan–Meier survival curves in subgroup analyses according to sex, age, grade, stage. (A. sex (P < 0.005); B. grade (P < 0.005); C. stage (P≤0.054); D. age (P < 0.005)) (E), (F), (G), (H). Functional analysis between Cup^{low}/TME^{high} and responder of patients under immunotherapy. (E. down in Cup^{low}/TME^{high}; F. down in responders; G. up in Cup^{low}/TME^{high}; H. up in responders. Each small polygon corresponds to a single KEGG pathway, and the size correlates with the ratio between the subgroups. Proteomaps (https://bionic-vis.biologie.uni-greifswald.de/)) (I). Kaplan-Meier overall survival curves of the independent validation GEO cohort (n = 171) stratified into three different subgroups based upon the Cup-TME classifier (Cup^{low}/TME^{high}, Mixed, Cup^{high}/TME^{low}). Log-rank test, P < 0 0.001.

3.7. Clinical features among Cup -TME classifier

We next investigated clinical features inside the Cup-TME classifier. The Kaplan–Meier survival curve uncovered that patients with Cup^{high}/TME^{low} had shorter survival. Our analysis provides further evidence that our classifier performed well in various clinical subtypes (Fig. 6 A, B, C, D). The validation set from the GEO cohort (we combined GSE42743 and GSE31056 as one group, used the remove BatchEffect function of the limma package in the R software to remove batch effects) was split into three groups, Cup^{low}/TME^{high}, mixed and Cup^{high}/TME^{low}, regarding the mean cut-off value of Cup_score and TME_score. Likewise, the classifier showed a statistically significant prognostic value in the validation cohorts. (Fig. 6 I).

4. Discussion

Known as a new form of programmed cell death, Cuproptosis involves lipoylated TCA cycle proteins and excessive copper accumulation [9]. A variety of diseases can be caused by disrupted Cu homeostasis. This substance is deemed to overpower the body's anti-oxidant systems, leading to protein modifications, DNA damage and lipid peroxidation. Of note, copper, a pivotal role in the progression of cancer, has been recognized by existing research. According to previous research, copper influences cancer progression through several pathways, including cancer angiogenesis, proliferation, and metastasis are key points during the process. The copper in the body is essential for immune response, but excessive amounts of copper can impair immunological activity [5–8]. Copper is important for cellular and humoral immunity. PD-L1 expression is modulated by intratumoral copper, which contributes to tumor-specific exhaustion of T cells and induces tumor immune evasion. Some Cups, like PSMB5, were reported to have a high expression in breast cancer tissue and M2 macrophages. Wang et al. experimentally demonstrated that PSMB5 contained immuno-suppressive and oncogenic characteristics [39]. SLC25A5 belongs to the SLC family (SLCs). Both infinitely proliferating tumor cells and activated immune cells require metabolic reprogramming and the expression of SLCs to uptake adequate nutrients and maintain homeostasis in the intracellular environment. In recent years, a growing number of studies have also shown that SLCs play an important regulatory role in tumor immunity [40]. Nachef et al. found the SLC7A5 are important for cancer cell's metabolism, growth, and proliferation. Moreover, most genes are closely related to mitochondrial metabolism and angiogenesis. We assumed these might build the pathological mechanisms behind suppressing the tumor immune microenvironment. Likewise, our results suggested that a high Cup_score HNSC represents overexpression of cell adhesion, metastasis, and immune evasion. We also explored immunocyte infiltration with several immune cells being various between the low and high Cuproptosis HNSC. These results allowed us to identify other potential ligand-receptor interactions between high/low Cuproptosis neoplastic cells and HNSC immune cells. Potential inter-cellular communication mechanisms include CD74+CXCR4DGHFGDG, TNFSF13B-TNFRSF13B, TNFSF13B-TNFRSF13C, and SPP1-CD44. In a word, Cuproptosis may affect tumor progression by connecting HNSC and immunocyte infiltration.

Since HNSC is heterogeneous, accurate prognostic indicators are crucial. There has been an increase in attention to molecular prognostic markers, which may provide effective complements to traditional clinicopathological parameters. Ultimately, we revealed 14 genes accompanying the HNSC patients' prognosis. We also selected 5 TME cells. We constructed a new prognostic model that united 14 Cuproptosis-related genes and 6 TME cells. Furthermore, imparity in the survival of HNSC patients between different score groups were observed. Furthermore, Cox analysis displayed that the classifier is an independent prognostic factor. Cup^{low}/TME^{high} patients had the best prognosis and clinical outcomes, suggesting Cuproptosis TMEs might show some shared character in the patient's antitumor immune.

Interestingly, Of the 22 TME cell types, Eosinophils, Mast cell and M2 macrophages have a poor prognosis in the HNSC cohorts studied. The prognostic value of Tumor-associated mast cells (TAMCs) is currently highly debated and remains unclear. However, it is well known that MCs can inhibit tumor growth, promote inflammation and induce tumor cell death by releasing TNF-α, IL-4, TGF-β, IL-1, MCP-3, IFN-γ and chymotrypsin. Notably, the effect of TAMCs cells seems to vary in different cancer types. Surprisingly, Treg cells, long thought to suppress antitumor immunotherapy, are a favorable prognostic indicator in the HNSC cohort. Recent research has reported that Treg cells can also further differentiate into three phenotypes, and not all types of Treg cells are immunosuppressive and even have antitumor activity. Admittedly, what we have observed in this study is far from complete and requires further research [41, 42].

Moreover, an exciting result indicates that plenty of immune checkpoint genes were overexpressed in the Cup^{low}/TME^{high} subgroup, suggesting that after experiencing immune checkpoint blockade, the Cup^{low}/TME^{high} subgroup could have a more robust antitumor immune response [43]. This demonstrates the Cuproptosis-TME classifier could be used to stratification cancer patients before immunotherapy. In addition, we questioned the role of tumor mutational burden in this classifier, but no significant differences exist between these subgroups. We found that the Cup^{low}/TME^{high}/TMB^{low} had a better prognosis than the Cup^{low}/TME^{high}/TMB^{high} subtype in the HNSC cohort. This phenomenon suggests that Tumor Mutation Burden is related to survival. We assume that the difference in subgroups is associated with immune activities or immune cell infiltration densities [44]. The lack of correlation between TMB and Cup-TME classifier implies that Regardless of TMB, classifiers can predict patient responses to immunotherapy.

There were some limitations to this study as well. It would have been helpful if experiments were conducted to verify how Cuproptosis regulated HNSC cells' behavior. Also, the practicality of the prognostic model should be tested with a multicenter clinical cohort.

In conclusion, Cuproptosis-related genes were thoroughly analyzed, including their effects on the immune microenvironment, clinical pathological characteristics, and prognosis. We created a Cup TME risk model and researched the susceptibility to anti-tumor medications. To our knowledge, this is the first paper to analyze the effectiveness of the combination of Cuproptosis and TME in the HNSC. Our research can be used to develop precision treatment plans for people with various HNSC subtypes.

Author contribution statement

Tingting Shu: Analyzed and interpreted the data; Wrote the paper. Xudong Wang: Conceived and designed the experiments; Analyzed and interpreted the data.

Funding

Ethics approval and consent to participate

Not applicable.

Availability of data and materials

The datasets during the current study are available in the Genomic Data Commons (GDC, https://gdc-portal.nci.nih.gov/legacy-archive/), Gene Expression Omnibus (GEO, https://www.ncbi.nlm.nih.gov/geo/), Cancer Therapeutics Response Portal (CTRP v.2.0, https://portals. broadinstitute.org/ctrp).

Declaration of competing interest

The authors declare that they have no known competing financial interests or personal relationships that could have appeared to influence the work reported in this paper.

Acknowledgments

Appendix A. Supplementary data

Supplementary data to this article can be found online at https://doi.org/10.1016/j.heliyon.2023.e15494.

References

[1] H. Sung, J. Ferlay, R.L. Siegel, M. Laversanne, I. Soerjomataram, A. Jemal, et al., Global cancer statistics 2020: GLOBOCAN estimates of incidence and mortality worldwide for 36 cancers in 185 countries, CA A Cancer J. Clin. 71 (3) (2021) 209–249, https://doi.org/10.3322/caac.21660.

[2] L.Q.M. Chow, Head and neck cancer, N. Engl. J. Med. 382 (1) (2020) 60–72, https://doi.org/10.1056/NEJMra1715715.

[3] T.Y. Seiwert, B. Burtness, R. Mehra, J. Weiss, R. Berger, J.P. Eder, et al., Safety and clinical activity of pembrolizumab for treatment of recurrent or metastatic squamous cell carcinoma of the head and neck (KEYNOTE-012): an open-label, multicentre, phase 1b trial, Lancet Oncol. 17 (7) (2016) 956–965, https://doi.org/10.1016/s1470-2045(16)30066-3.

[4] P. Economopoulou, C. Perisanidis, E.I. Giotakis, A. Psyrri, The emerging role of immunotherapy in head and neck squamous cell carcinoma (HNSCC): anti-tumor immunity and clinical applications, Ann. Transl. Med. 4 (9) (2016) 173, https://doi.org/10.21037/atm.2016.03.34.

[5] E.J. Ge, A.I. Bush, A. Casini, P.A. Cobine, J.R. Cross, G.M. DeNicola, et al., Connecting copper and cancer: from transition metal signalling to metalloplasia, Nat. Rev. Cancer 22 (2) (2022) 102–113, https://doi.org/10.1038/s41568-021-00417-2.

[6] B.-E. Kim, T. Nevitt, D.J. Thiele, Mechanisms for copper acquisition, distribution and regulation, Nat. Chem. Biol. 4 (3) (2008) 176–185, https://doi.org/10.1038/nchembio.72.

[7] S. Lutsenko, Human copper homeostasis: a network of interconnected pathways, Curr. Opin. Chem. Biol. 14 (2) (2010) 211–217, https://doi.org/10.1016/j.cbpa.2010.01.003.

[8] T.D. Rae, P.J. Schmidt, R.A. Pufahl, V.C. Culotta, T.V. O'Halloran, Undetectable intracellular free copper: the requirement of a copper chaperone for superoxide dismutase, Science (New York, NY) 284 (5415) (1999) 805–808, https://doi.org/10.1126/science.284.5415.805.

[9] P. Tsvetkov, S. Coy, B. Petrova, M. Dreishpoon, A. Verma, M. Abdusamad, et al., Copper induces cell death by targeting lipoylated TCA cycle proteins, Science (New York, NY) 375 (6586) (2022) 1254–1261, https://doi.org/10.1126/science.abf0529.

[10] S. Tang, L. Zhao, X.B. Wu, Z. Wang, L.Y. Cai, D. Pan, et al., Identification of a novel cuproptosis-related gene signature for prognostic implication in head and neck squamous carcinomas, Cancers 14 (16) (2022), https://doi.org/10.3390/cancers14163986.

[11] A.M. Newman, C.L. Liu, M.R. Green, A.J. Gentles, W. Feng, Y. Xu, et al., Robust enumeration of cell subsets from tissue expression profiles, Nat. Methods 12 (5) (2015) 453–457, https://doi.org/10.1038/nmeth.3337.

[12] D. Zeng, Z. Ye, J. Wu, R. Zhou, X. Fan, G. Wang, et al., Macrophage correlates with immunophenotype and predicts anti-PD-L1 response of urothelial cancer, Theranostics 10 (15) (2020) 7002–7014, https://doi.org/10.7150/thno.46176.

[13] S. Chen, Y. Gao, Y. Wang, T. Daemen, The combined signatures of hypoxia and cellular landscape provides a prognostic and therapeutic biomarker in hepatitis B virus-related hepatocellular carcinoma, Int. J. Cancer 151 (5) (2022) 809–824, https://doi.org/10.1002/ijc.34045.

[14] M. Carlson, S. Falcon, H. Pages, N. Li, org. Hs. eg. db: genome wide annotation for Human, R package version 3 (2) (2019) 3, https://doi.org/10.18129/B9.bioc.

[15] T. Wu, E. Hu, S. Xu, M. Chen, P. Guo, Z. Dai, et al., clusterProfiler 4.0: a universal enrichment tool for interpreting omics data, Innovation 2 (3) (2021), 100141, https://doi.org/10.1016/j.xinn.2021.100141.

[16] G. Yu, L.-G. Wang, Y. Han, Q.-Y. He, clusterProfiler: an R package for comparing biological themes among gene clusters, OMICS A J. Integr. Biol. 16 (5) (2012) 284–287, https://doi.org/10.1089/omi.2011.0118.

[17] G. Korotkevich, V. Sukhov, N. Budin, B. Shpak, M.N. Artyomov, A. Sergushichev, Fast gene set enrichment analysis, bioRxiv (2021), 060012, https://doi.org/10.1101/060012.

[18] P. Langfelder, S. Horvath, WGCNA: an R package for weighted correlation network analysis, BMC Bioinf. 9 (1) (2008) 1–13, https://doi.org/10.1186/1471-2105-9-559.

[19] B. Zhang, S. Horvath, A general framework for weighted gene co-expression network analysis, Stat. Appl. Genet. Mol. Biol. 4 (1) (2005), https://doi.org/10.2202/1544-6115.1128.

[20] R. Saito, M.E. Smoot, K. Ono, J. Ruscheinski, P.L. Wang, S. Lotia, et al., A travel guide to Cytoscape plugins, Nat. Methods 9 (11) (2012) 1069–1076, https://doi.org/10.1038/nmeth.2212.

[21] Z. Gu, R. Eils, M. Schlesner, Complex heatmaps reveal patterns and correlations in multidimensional genomic data, Bioinformatics 32 (18) (2016) 2847–2849, https://doi.org/10.1093/bioinformatics/btw313.

[22] M.E. Ritchie, B. Phipson, D. Wu, Y. Hu, C.W. Law, W. Shi, et al., Limma powers differential expression analyses for RNA-sequencing and microarray studies, Nucleic Acids Res. 43 (7) (2015) e47, https://doi.org/10.1093/nar/gkv007, e.

[23] S. Jin, C.F. Guerrero-Juarez, L. Zhang, I. Chang, R. Ramos, C.-H. Kuan, et al., Inference and analysis of cell-cell communication using CellChat, Nat. Commun. 12 (1) (2021) 1–20, https://doi.org/10.1038/s41467-021-21246-9.

[24] J. Fu, K. Li, W. Zhang, C. Wan, J. Zhang, P. Jiang, et al., Large-scale public data reuse to model immunotherapy response and resistance, Genome Med. 12 (1) (2020) 21, https://doi.org/10.1186/s13073-020-0721-z.

[25] D. Maeser, R.F. Gruener, R.S. Huang, oncoPredict: an R package for predicting in vivo or cancer patient drug response and biomarkers from cell line screening data, Briefings Bioinf. 22 (6) (2021) bbab260, https://doi.org/10.1093/bib/bbab260.

[26] H. Wickham, Data Analysis, Springer, 2016, pp. 189–201, ggplot2.

[27] J. Chen, J. Zhou, J. Lu, H. Xiong, X. Shi, L. Gong, Significance of CD44 expression in head and neck cancer: a systemic review and meta-analysis, BMC Cancer 14 (2014) 15, https://doi.org/10.1186/1471-2407-14-15.

[28] C. He, L. Sheng, D. Pan, S. Jiang, L. Ding, X. Ma, et al., Single-cell transcriptomic analysis revealed a critical role of SPP1/CD44-mediated crosstalk between macrophages and cancer cells in glioma, Front. Cell Dev. Biol. 9 (2021) 779319, https://doi.org/10.3389/fcell.2021.779319.

[29] X. Ji, Y. Liu, F. Mei, X. Li, M. Zhang, B. Yao, et al., SPP1 overexpression is associated with poor outcomes in ALK fusion lung cancer patients without receiving targeted therapy, Sci. Rep. 11 (1) (2021), 14031, https://doi.org/10.1038/s41598-021-93484-2.

[30] J. Qi, H. Sun, Y. Zhang, Z. Wang, Z. Xun, Z. Li, et al., Single-cell and spatial analysis reveal interaction of FAP+ fibroblasts and SPP1+ macrophages in colorectal cancer, Nat. Commun. 13 (1) (2022) 1742, https://doi.org/10.1038/s41467-022-29366-6.

[31] M. Binnewies, E.W. Roberts, K. Kersten, V. Chan, D.F. Fearon, M. Merad, et al., Understanding the tumor immune microenvironment (TIME) for effective therapy, Nat. Med. 24 (5) (2018) 541–550, https://doi.org/10.1038/s41591-018-0014-x.

[32] P. Economopoulou, I. Kotsantis, A. Psyrri, Tumor microenvironment and immunotherapy response in head and neck cancer, Cancers 12 (11) (2020) 3377, https://doi.org/10.3390/cancers12113377.

[33] J.G. Egen, W. Ouyang, L.C. Wu, Human anti-tumor immunity: insights from immunotherapy clinical trials, Immunity 52 (1) (2020) 36–54, https://doi.org/10.1016/j.immuni.2019.12.010.

[34] R.L. Ferris, Immunology and immunotherapy of head and neck cancer, J. Clin. Oncol. 33 (29) (2015) 3293–3304, https://doi.org/10.1200/JCO.2015.61.1509.

[35] P.S. Hegde, D.S. Chen, Top 10 challenges in cancer immunotherapy, Immunity 52 (1) (2020) 17–35, https://doi.org/10.1016/j.immuni.2019.12.011.

[36] Y. Zhou, B. Zhou, L. Pache, M. Chang, A.H. Khodabakhshi, O. Tanaseichuk, et al., Metascape provides a biologist-oriented resource for the analysis of systems-level datasets, Nat. Commun. 10 (1) (2019) 1523, https://doi.org/10.1038/s41467-019-09234-6.

[37] I. Micaily, J. Johnson, A. Argiris, An update on angiogenesis targeting in head and neck squamous cell carcinoma, Cancers Head Neck 5 (1) (2020) 1–7, https://doi.org/10.1186/s41199-020-00051-9.

[38] L. Xu, C. Deng, B. Pang, X. Zhang, W. Liu, G. Liao, et al., TIP: a web server for resolving tumor immunophenotype ProfilingTIP: tracking tumor immunophenotype, Cancer Res. 78 (23) (2018) 6575–6580.

[39] C.Y. Wang, C.Y. Li, H.P. Hsu, C.Y. Cho, M.C. Yen, T.Y. Weng, et al., PSMB5 plays a dual role in cancer development and immunosuppression, Am. J. Cancer Res. 7 (11) (2017) 2103–2120.

[40] R. Chen, L. Chen, Solute carrier transporters: emerging central players in tumour immunotherapy, Trends Cell Biol. 32 (3) (2022) 186–201, https://doi.org/10.1016/j.tcb.2021.08.002.

[41] T. Maj, W. Wang, J. Crespo, H. Zhang, W. Wang, S. Wei, et al., Oxidative stress controls regulatory T cell apoptosis and suppressor activity and PD-L1-blockade resistance in tumor, Nat. Immunol. 18 (12) (2017) 1332–1341, https://doi.org/10.1038/ni.3868.

[42] T. Saito, H. Nishikawa, H. Wada, Y. Nagano, D. Sugiyama, K. Atarashi, et al., Two FOXP3(+)CD4(+) T cell subpopulations distinctly control the prognosis of colorectal cancers, Nat. Med. 22 (6) (2016) 679–684, https://doi.org/10.1038/nm.4086.

[43] L. Liu, M.A. Lim, S.N. Jung, C. Oh, H.R. Won, Y.L. Jin, et al., The effect of Curcumin on multi-level immune checkpoint blockade and T cell dysfunction in head and neck cancer, Phytomedicine : Int. J. Phytother. Phytopharmacol. 92 (2021), 153758, https://doi.org/10.1016/j.phymed.2021.153758.

[44] X. Wang, M. Li, Correlate tumor mutation burden with immune signatures in human cancers, BMC Immunol. 20 (1) (2019) 4, https://doi.org/10.1186/s12865-018-0285-5.